Appl. Phys. A 73, 347–355 (2001) / Digital Object Identifier (DOI) 10.1007/s003390100736

Applied Physics A
Materials
Science & Processing

Comparison of fractal analyses methods and fractal dimension for pre-treated stainless steel surfaces and the correlation to adhesive joint strength

A. Mannelqvist[1,*], **M. Ring Groth**[2]

[1] Department of Physics, Luleå University of Technology, 971 87 Luleå, Sweden
(Fax: +46-920/91074, E-mail: manne@mt.luth.se)
[2] Department of Materials and Manufacturing Engineering, Luleå University of Technology, 971 87 Luleå, Sweden

Received: 22 December 1999/Accepted: 9 October 2000/Published online: 9 February 2001 –

Abstract. The fractal dimensions of six differently mechanically pre-treated stainless steel samples were investigated using five fractal algorithms. The surfaces were analyzed using a profiler, atomic force microscopy (AFM), scanning electron microscopy (SEM) and light microscopy (LM), and thereafter adhesively bonded and tested in single-overlap joints to test their tensile strength. All samples showed different fractal behavior, depending on the microscopic methods and fractal algorithms. However, the overall relation between fractal dimension and tensile strength is qualitatively the same, except for the SEM images. This verifies that tensile strength is correlated to fractal dimension, although only within the length-scale of the profiler and the light microscope (≈ 0.5–$100\,\mu$m). The AFM method was excluded in this comparison, since the limitation in the z-direction for the AFM scanner made it difficult to scan the rougher parts of the blasted samples. The magnitude of the surfaces is a parameter not often considered in fractal analysis. It is shown that the magnitude, for the Fourier method, is correlated to the arithmetic average difference, R_a, but only weakly to the fractal dimension. Hence, traditional parameters, such as R_a, tell us very little about the spatial distribution of the elevation data.

PACS: 68.35.Bs; 68.35.Ct; 68.35.Gy

The complex bonding properties of an adhesive and a substrate can be explained by theories such as physical adsorption, chemical bonding, electrostatic attraction, mechanical interlocking and weak-boundary-layer theory [1]. Different surface treatments of a substrate may introduce electric dipoles on the surface resulting in increased Van der Waals forces, the removal of weak layers, and increased surface roughness.

The change in surface roughness and geometry may lead to increased mechanical interlocking, surface area, and wettability. The correlation between surface roughness and adhesive strength is not well understood, and surfaces possessing equal surface roughness and surface area can have different adhesive strengths. One explanation is that the strength of a single joint is not related to the bonded area. By inserting non-bonding material (polypropylene) into the single-joint laps, Wang et al. [1] showed weak, or no, correlation between bonded area and adhesive strength. This behavior can be explained by the stress distribution within the joint, where the adherent, often with a low Young's modulus compared to the substrate, will experience the greatest stress at the edges of the joints [1].

Measuring and characterizing surface roughness plays an important role in many fields of material science and there have been many attempts to quantify and unify the measurements of surface roughness. Traditional methods such as standard deviation, slope and curvature are easy to understand and calculate but can only be used for qualitative investigations as they differ by scale of measurement. They also tell us little about the spatial distribution of the topography.

The use of fractal geometry, with concepts such as self-similarity and self-affinity, introduced by Mandelbrot, has changed and broadened the characterization of surfaces and profiles and of many phenomena and processes. Unlike Euclidean geometry, fractal geometry has a dimension that is non-integral and is independent of the scale of measurement. The fractal dimension, D, is restricted by $2 < D < 3$, whereas Euclidean (flat) surfaces have $D = 2$. For real surfaces, the fractal dimension is naturally limited to a certain range of length-scales. However, metal surfaces treated with processes such as corrosion and blasting, show scale invariance in many decades and can be characterized by fractal analyses. Even machined surfaces, intended to mimic smooth Euclidean geometry, show chaotic behavior that can be characterized by fractal geometry [2].

It has been reported that the fractal dimension of a Fe-alloy surface depends on the exposure time to a corrosive solution [3]. Other studies by Shigeyasu et al. [4] concluded that grit-blasted pre-treated steel surfaces possess fractal characteristics, and that maximum adhesive strength was correlated to maximum fractal dimension. They also concluded that fractal dimension varied with the blasting angle, in contrast

*Corresponding author.

to the arithmetic average difference, R_a, that stayed almost constant.

The contact angle, θ_t, a property connected to adhesion and wettability, was shown by Hazlett [5] to be correlated as:

$$\cos(\theta_t) = \left(\frac{L}{l}\right)^{D-2} \cos(\theta)\,, \tag{1}$$

where L is the upper limit of fractal behavior, l is the lower limit, D the fractal dimension and θ is the contact angle for a flat surface. The factor $(L/l)^{D-2}$ is defined as the roughness factor and correlates the contact angle for a flat surface with a fractal surface. It is also assumed that:

(i) l is much larger than the molecule size;
(ii) L is much smaller than the diameter of a liquid droplet;
(iii) the interfacial tension of a solid is isotropic and independent of crystal orientation [6].

This relation is of course only valid for angles where the right-hand side of the equation is smaller then unity. For adhesives having a contact angle less than 90° (i.e. most of them), the wettability will increase in proportion to the fractal dimension. In contrast, for surfaces having contact angles greater than 90°, the wettability will decrease in proportion to the fractal dimension. Shibuichi et al. [7] reported a contact angle larger than 170°, without fluorination treatments, for fractal alkylketene dimer surfaces, with a fractal dimension of $D \approx 2.30$, compared to a contact angle of 109° for a flat surface ($D \approx 2$).

This paper compares different fractal analyses methods for pre-treated steel surfaces and correlates fractal dimension to tensile strength for single-overlap joints. The samples were treated by five erosion treatments, brushing or blasting, and the surfaces were evaluated with different microscopic methods and fractal algorithms. The fractal analysis is motivated by the assumption that a superposition of a random set of events and/or power-law distributions will generate fractals [8], an assumption that should be valid for the pre-treated steel samples at certain length-scales.

1 Fractal analysis

There are numerous algorithms available to calculate the fractal dimension from elevation data obtained from profilers, interferometers, scanning probe microscopes (SPM) and other topographical methods. All these methods produce single-valued profiles, which cannot reveal overhangs and are self-affine rather than self-similar. Self-affine data do not scale the same laterally as vertically, as the self-similar Koch curve shown in many fractal textbooks.

Among the most popular algorithms for self-affine profiles are the Minkowski plot (a variation of the Richardson plot), variance methods (root-mean-square, rms), Hurst, structure function, box counting, integrated fast-Fourier transforms, and the regular fast-Fourier-transform method [8–13].

These methods can also be applied to surfaces since they can be seen as built up of profiles, as for SPM images. But there are, however, also specific surface algorithms such as the area–perimeter method and the Korsak plot that can be used [8]. The relationship between the fractal dimension obtained from a profile and its surface is $D_{surface} = D_{profile} + 1$ for a statistically isotropic surface [14]. Many algorithms have been tested on simulated fractal profiles and surfaces to test their precision and accuracy [8, 15], and it is clear that the calculated fractal values vary between the different algorithms and test samples. The highest precision has, however, been shown for lower fractal dimensions, i.e. $1 < D < 1.3$ for profiles and $2 < D < 2.3$ for surfaces [8, 16, 17]. There have also been attempts to calibrate these algorithms on simulated surfaces [16], but the question remains: how well does the simulated surface coincide with the real surface? Real surfaces may be anisotropic, include noise and mixed, random and ordered, processes. They may also have a limited scale invariance and fractal behavior, making some of the fractal algorithms more suitable to use.

1.1 Fractal analysis of SEM and LM images

Fractal analysis of a surface is usually performed on surface-elevation data, limiting the use of scattering techniques such as SEM and LM. However, the scattering of light from a fractal surface is itself fractal, and the images may be characterized by texture methods, relating brightness and spatial organization, making it possible to compare image textures qualitatively. We have used a texture method described by Russ [8] where the brightness difference for a given distance is plotted versus pixel distance in a log–log plot. The slope of the curve is an indicator of surface texture, and does not directly correspond to the fractal dimension. However, under the same light and viewing conditions, qualitative data can be used to range the surfaces.

A less convenient method is to cut the sample in slices and view the profiles with a SEM (or LM if the resolution permits). Since the profiles or contours are not single-valued, none of the fast-Fourier, rms, or Hurst methods could be used. However, by digitizing the profile pictures and adding them together to one profile, the total length, L, of the profile can be measured for different measuring sticks, ε. If the length is plotted versus ε in a log–log plot, (so-called Richardson plot), the slope, and hence the fractal dimension, D, can be calculated from

$$L(\varepsilon) = F \cdot \varepsilon^{(1-D)}\,, \tag{2}$$

where F is a constant, related to the magnitude of the profile. The obtained fractal dimension is equal to the so-called Hausdorff–Besicovitch dimension.

1.2 Fractal analysis of profiles and AFM images

To evaluate topographic data from the profiler, we have chosen the fast-Fourier-transform method, a rms method and the Hurst method. These methods, excluding the Hurst method, have also been applied to AFM images.

The Fourier method is fast, straightforward and has the advantage of revealing underlying waviness, regular patterns and noise that sometimes can be removed.

The fractal dimension, D, can be evaluated from plotting the power spectra

$$P(\omega) = B \cdot \omega^{-\beta} \tag{3}$$

in a log–log plot. The fractal dimension, D, is calculated from $D = (5 - \beta)/2$, where β is the slope, ω is the frequency and B is a constant related to the magnitude of the fractal profile [19, 20].

The intercept in the log–log plot, $\log(B)$, provides valuable information about the magnitude of the sample surface. Two surfaces with the same fractal dimension but with different intercepts can exhibit large differences in topography, and should be characterized differently. Therefore, both the fractal dimension and intercept should be used to characterize a surface. This explains why traditional roughness measurements, such as R_a or the *rms* value, cannot be used alone, since these are both linked to the magnitude and to the spatial distribution of the topography.

R_a and *rms* for a profile, y, are defined as:

$$R_a = \frac{1}{N-1}\sum_{i=1}^{N}|y_i - \overline{y}| \tag{4}$$

$$rms = \sqrt{\frac{1}{N-1}\sum_{i=1}^{N}(y_i - \overline{y})^2}\,, \tag{5}$$

respectively, where $\overline{y}$ is the profile average and N is the number of data points in the set.

Church [18] has derived the relationship between the *rms*/standard deviation, σ^2, and the parameters used to define the power spectra for a fractal profile, B and β. The relation is:

$$\sigma^2 = \frac{BL^{-(\beta+1)}}{-(\beta+1)}\,, \tag{6}$$

where L is the total length of the measured profile. This equation emphasizes that the *rms*/standard deviation values are scale dependent. Other parameters, such as the topothesy, have been suggested to characterize the magnitude. The topothesy is defined as:

$$\Lambda^{3+\beta} = B\frac{(2\pi)^{-\beta}}{2\Gamma(-\beta)\cos(-\beta\pi/2)}\,, \tag{7}$$

where Λ is the mean distance between two points having a slope of 1 rad [3]. This distance can be short, often less than the resolution of the instrument or the atomic spacing of the sample. A physical interpretation of the results could therefore be difficult to give, hence limiting the usability of the technique.

The *rms*/variance method is useful since it combines traditional roughness measurements with fractal analyses, and emphasizes the fact that *rms*/variance values are scale dependent and can only be used as qualitative measurements. The fractal dimension is obtained from the log–log plot of the *rms*/variance values versus the perimeter length or box size. In this study we divide the profiles or the surfaces into equal-sized lengths or boxes, and calculate the variance or the square of the *rms*, σ^2, as:

$$\sigma^2(B) = \left\langle \frac{1}{B^2 - 1}\sum_{i=1}^{B^2}(z_i - \overline{z})^2 \right\rangle, \tag{8}$$

where B^2 is the number of data points in one length or box, z_i is the height at each point, $\overline{z}$ is the average height for a length or box, and $\langle \ldots \rangle$ denotes an average over all non-overlapping lengths or boxes covering the total profile or surface. The fractal dimension of a profile correlates to the slope as $D = 2 - \beta$ for the variance, and as $D = 2 - 2\beta$ for the *rms* values.

The Hurst (or the R/S) method is a simple and straightforward method to apply on self-affine profile data. Hurst developed the method when studying the Nile River and problems related to water storage, and it was originally designed for time-based data [19]. The method finds the greatest difference, $R(\tau)$, within a 'window', τ, and displays the difference in a log–log plot as a function of 'window' width, according to

$$R(\tau) = {}_{1<t<\tau}^{\max} X(t, \tau) - {}_{1<t<\tau}^{\min} X(t, \tau)\,, \tag{9}$$

where $X(t, \tau)$ is the data set. By dividing $R(\tau)$ by the standard deviation, $S(\tau)$, the R/S value will be a dimensionless number that can be used to compare different phenomena and data sets. The slope, H, will give the fractal dimension according to $D = 2 - H$. A drawback with this method, however, is that transient noise may hide 'real' data, although when tested on simulated isotropic noise-free profiles, the Hurst method proves to be one of the more accurate methods [8].

1.3 Summary of methods

The following microscopic methods and fractal algorithms were used to derive the fractal dimensions from the samples:

Microscopic method	Fractal algorithm
Profiler	Fourier, *rms* and Hurst
AFM	Fourier, *rms*
SEM	Texture, Richardson
LM	Texture

Also:

(i) the intercepts from the Fourier method on profiles were used to show the connection between the magnitude and the R_a value for the surfaces;
(ii) the roughness factor was calculated from the Hurst method on profiles and correlated to tensile strength.

2 Experimental

2.1 Preparation of stainless steel surfaces and subsequent bonding

The most commonly used materials in metal adhesive bonding are aluminum alloys and other light alloys. An increased use of adhesive bonding as a joining method is, however, seen for ferrous alloys, e.g. stainless steel. Stainless steel has unique surface properties among the ferrous alloys as the surface spontaneously forms a stable oxide in any oxidizing media, such as air or water. If the surface is also mechanically treated there will be a change both in morphology and chemical composition of the surface, depending on the technique involved. Different abrasive media can transport material to the surface and thus influence the composition of the newly formed passive layer. The most obvious difference will, however, be the change in morphology and hence the

surface roughness. The material used in this investigation was a common austenitic stainless steel, AISI 304 with an ordinary surface quality.

Six degreasing and mechanical treatments were utilized, degreasing being the simpler. Then a variety of abrasive techniques were employed. The treatments are given in Table 1, together with typical data. On a macro-scale, the brushing and Scotch-Brite techniques do not alter the surface much compared to a non-treated surface.

The adherents were bonded with a room-temperature-curing 2-component epoxy, Araldite 2015 (Ciba-Geigy). Adhesive properties can be found in Table 2. The manufacturer recommends a curing time of at least 24 h. All joints were cured for at least 96 h before testing.

The joints were assembled as single-overlap joints, with an overlap width of 40 mm, and a 40-mm overlap. The adherend thickness was rather large, 4 mm, to minimize bending effects during the tensile lap-shear test. A bondline thickness of 0.4 mm was used. The adhesive layer thickness was controlled with a spacing wire within the adhesive joint. Excess adhesive in the form of spews or fillets was not taken away, but measures were taken so that each joint had roughly the same excess amount before clamping and curing.

The joints were tested according to ASTM D1002-94, with the exception of test-piece size and the results are shown in Fig. 1. The visible type of failure ranged from almost fully cohesive (water blasted) to almost completely interfacial (degreased). It can clearly be seen that any abrasion technique will have a positive influence on joint strength as measured by single lap-shear tests. The type of abrasion does not seem to have any major influence on the strength of the joint. However, the grit-blasting abrasion technique does give the highest strength with the least variation. Results similar to this have been reported earlier, and it has been shown that the type of abrasion influences durability tests. This was not investigated in this study.

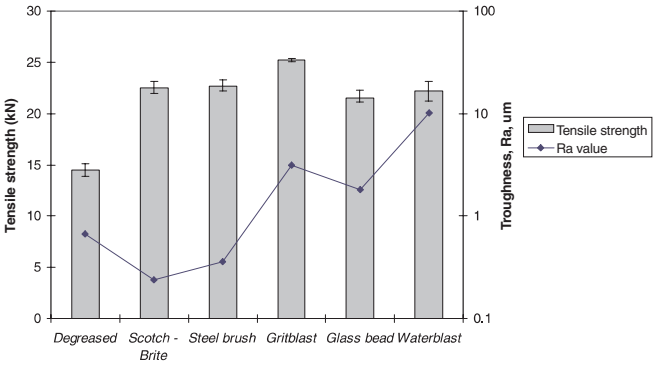

Fig. 1. Fracture loads (kN) for mechanically pre-treated adherents and their R_a values (μm)

3 Results and discussion

3.1 Profiler

3.1.1 Fourier method. All profiles where taken with a Pherten profiler, using a standard scan length of 4 mm and 5760 data points, resulting in a resolution of 0.394 μm. Each sample was scanned three times in two directions, 90° to each other, to reveal anisotropy, and the averages in fractal dimension were calculated. Figure 2 presents the variation in fractal dimension and tensile strength for the six samples, using the Fourier method.

Table 1. Pre-treatment methods and their characteristics

Pre-treatment method	Typical process/result	Notable data
Degreased by wiping with isopropanyl alcohol (Deg)	Manual wiping, waterbreak test	Lintfree cloth was used, waterbreak test used as a measure of cleanliness
Abraded with Scotch-Brite pads (Sct)	Manual process, random pattern	New pads for each surface, so as not to transfer particles between samples. Same abrasion time for all samples
Abraded with a steel brush (Ste)	Manual process, random pattern	Brush-cleaned between surfaces. Same abrasion time for all samples
Sandblasted (Gri)	Semi-manual process, blast angle kept constant	Surfaces cleaned manually, blast pressure and grit media kept constant
Glass-bead blasted (Gla)	Semi-manual process, blast angle kept constant	Surfaces cleaned manually, blast pressure and grit media kept constant
Water blasted (Wat)	Fully automated process, organized blasting pattern, blast angle kept constant	No abrasive media used. Waterblasting equipment could be programmed, and all surfaces were treated at the same time

Table 2. Adhesive properties for Araldite 2015 (as supplied by Ciba)

Tensile strength at 23 °C	Tensile modulus	Cure time, tensile strength > 10 MPa	Typical lap-shear strength on stainless steel, cure 16 h/40 °C
30 MPa	2 GPa	7 h @ 23 °C	19 MPa

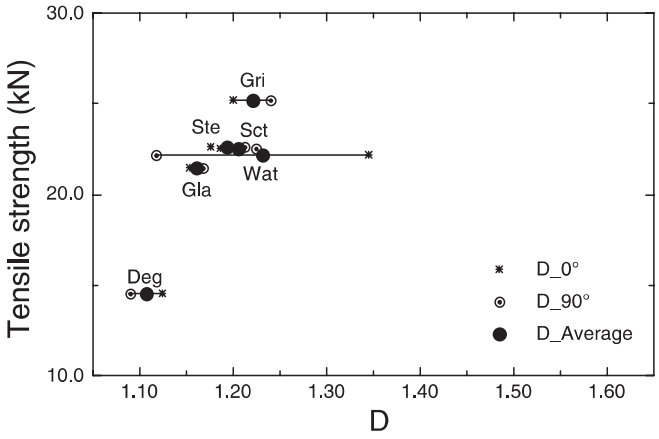

Fig. 2. Tensile strength versus fractal dimension, for the six surface-treated samples, calculated using the Fourier method on profiles. The abbreviations are given in Table 1. The data are for the two directions, 90° to each other, and for their average. The length of the horizontal bars reflects the directional differences in fractal dimension

The water-blasted sample shows an extensive difference in directionality compared with the other samples. It has a low fractal dimension in the 0° direction, comparable to the fractal dimension of the degreased surface, and a high fractal dimension in the 90° direction. These directional differences in surface roughness are also visible to the eye.

The assumption that tensile strength and fractal dimension are related may explain why the water-blasted surface shows a lower tensile strength than expected from the figure. If the stress field in the joint is mainly pointing in the direction of the lower fractal dimension, the joint will be less supportive than it would for the perpendicular direction with a higher fractal dimension.

As seen in Fig. 3, nearly all of the Fourier plots exhibited discrepancies at higher frequencies. These higher frequencies of 'bumps' had to be removed to give reasonable fractal values ($D \approx 1.0$). The reason for these 'bumps' is presumably the nature of the scanning procedure as the reciprocal of the frequency is in the order of the tip size, 1.5–2.5 μm.

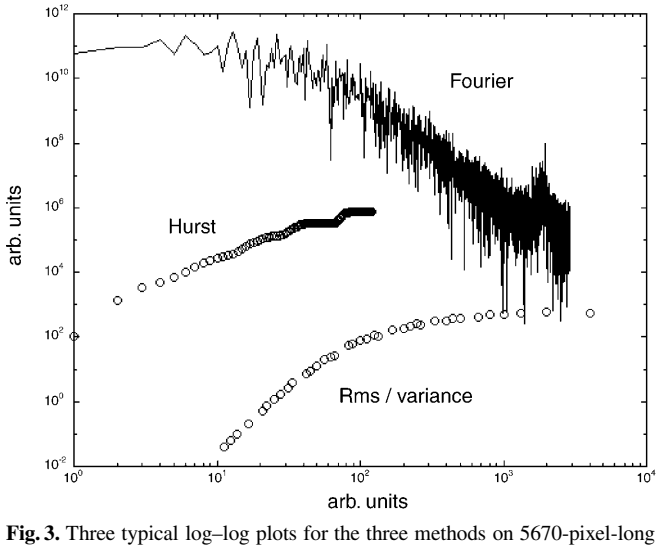

Fig. 3. Three typical log–log plots for the three methods on 5670-pixel-long profiles

Figure 3 also shows the difference in linearity between the profile methods and the difficulty in determining the fractal range. Three typical log–log plots from the grit-blasted sample are shown. The plots are normalized so neither the slope nor the intercept coincides with the original log–log plots.

3.1.2 Rms method. The *rms* method was not as simple to use, as it was difficult to outline a distinct fractal region with constant slope. Some typical *rms* plots are shown in Fig. 4. It has also been pointed out that the *rms* method could have a lower and an upper cutoff length close to each other. Sometimes as little as 10% of the plot may show a fractal behavior [14], making it difficult to determine the natural fractal cutoff.

However, the results in Fig. 5 show that the *rms* method gives a higher fractal dimension, 1.20–1.60, compared to the Fourier method, 1.10–1.35, and the relationship between tensile strength and fractal dimension is not distinct. The grit-blasted sample also showed a low value compared to the other samples and the directional differences for the water-blasted

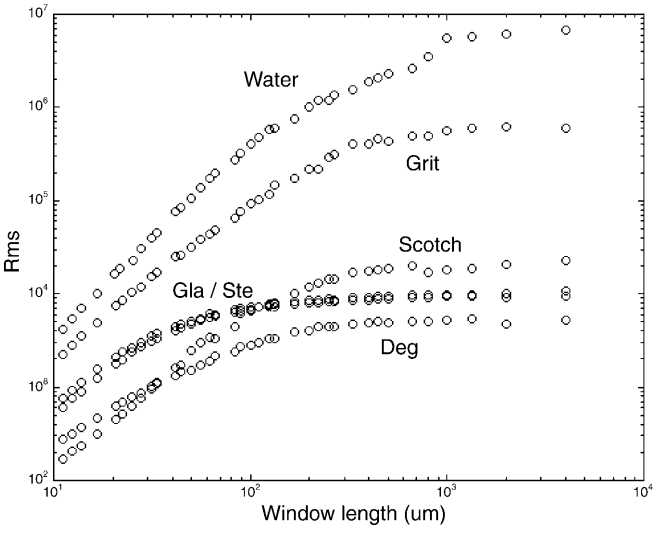

Fig. 4. Typical log–log plots for the *rms* method illustrating the differences in intercept and slope and the difficulty in determining a fractal region for some of the samples

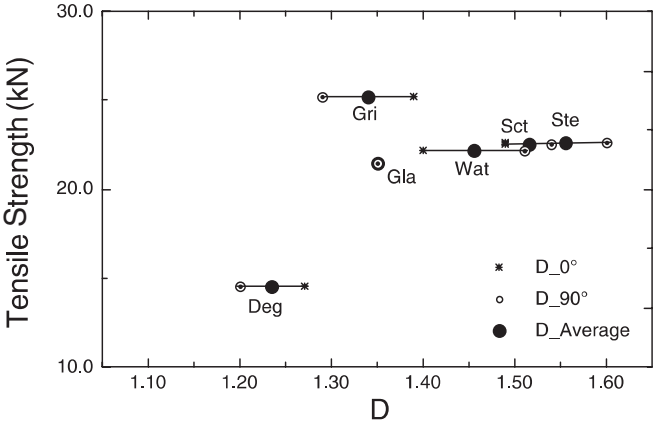

Fig. 5. Tensile strength versus fractal dimension for the six surface-treated samples, calculated using the *rms* method on profiles. The abbreviations are given in Table 1. The data are for the two directions, 90° to each other, and for their average. The lengths of the horizontal bars reflect the directional differences in fractal dimension

sample, seen using the Fourier method, were not revealed with the *rms* method.

3.1.3 Hurst method and the roughness factor. The Hurst method shown in Fig. 6 gave a mixed result between the Fourier and the *rms* method, still qualitatively connecting fractal dimension to tensile strength. The steel-brushed sample also showed some extraordinary directional differences, whereas the glass-blasted sample showed a higher relative fractal value than the other methods. However, the surfaces showed distinct fractal regions in the log–log plots, reducing the uncertainty in picking out the slope.

The roughness factor, $(L/l)^{D-2}$ in (1), was calculated from the fractal dimension and cutoff lengths (upper and lower limits for fractal behavior). The cutoff lengths varied in the range 1–80 μm for the samples and the calculated roughness factors are compared to tensile strength in Fig. 7. Qualitatively, the relation to tensile strength is roughly the same as in Fig. 6, hence relating the roughness factor (and wettability) to tensile strength of the surface. However, the change in wettability for the samples was not tested. As regards the cutoff length for the fractal behavior, there have been suggestions that the correlation length could be used to determine the upper limit. This is, however, not correct as the correlation length, i.e. the distance between successive crossings of a profile through some set level, turns out to be an artifact of the measurement procedure rather than a characteristic of the surface [21].

3.1.4 Intercept for the Fourier method. The relationship between the intercept in a log–log plot (the magnitude) and the R_a values from the six samples is clearly seen for the Fourier method in Fig. 8. No such relationship is seen for the fractal dimension, showing that R_a tells us very little about the spatial distribution of elevation data. The same behavior is observed for the *rms* method in Fig. 4, although the actual intercept is not shown in the plot. Figure 4 also shows the importance of giving both intercept and fractal dimension to characterize the surfaces, as two samples having the same slope but different intercept, show different topography.

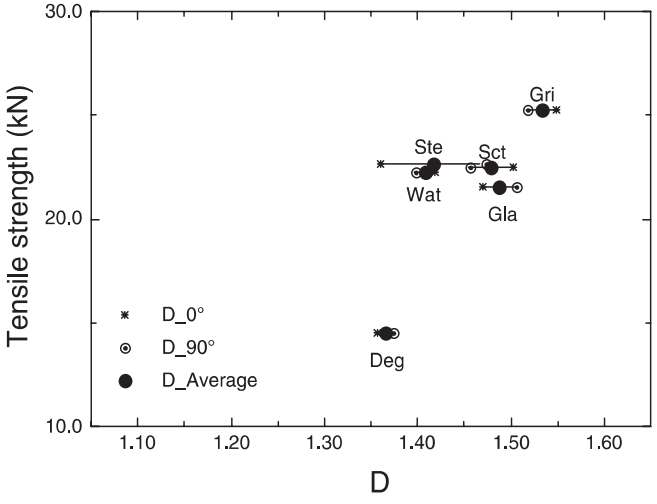

Fig. 6. Tensile strength versus fractal dimension for the six surface-treated samples, calculated using the Hurst method on profiles. Abbreviations are given in Table 1. The data are for the two directions, 90° to each other, and for their average. The lengths of the horizontal bars reflect the directional differences in fractal dimension

3.2 Light microscopy and SEM

The simplest method for evaluating surface-treated samples is probably the use of a light microscope, as the technique uses no special sample preparation. Images, with a magnification factor of 200, of the six samples are shown in Fig. 9. Figure 10 shows the relationship between tensile strength and texture calculated from the LM images. Every value is an average of four images. The texture values correspond to the slope in the log–log plot of the average pixel-brightness difference versus distance. Almost the same relationship between fractal dimension and tensile strength can be seen here as for profiles, especially for the Hurst method. This method is an easy and fast method to qualitatively compare different surfaces.

The same analysis on SEM images, taken with 800× and 2000× magnification, showed little fractal behavior and no relation to tensile strength. This is not surprising, as the images do not look fractal at that length-scale. The six samples, imaged by SEM at 800× magnification, are seen in Fig. 11.

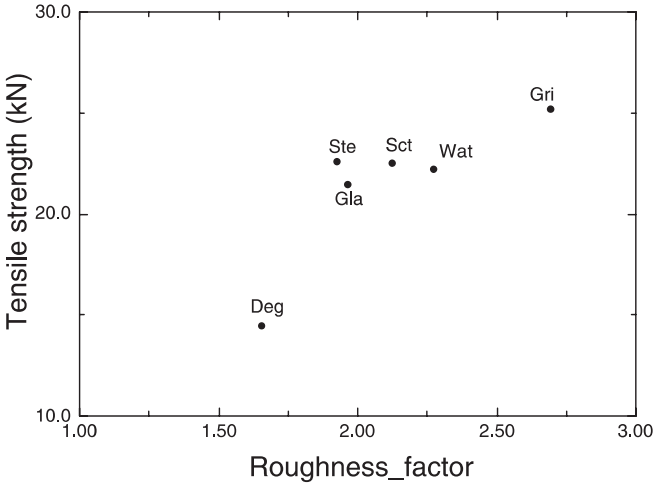

Fig. 7. Tensile strength versus the roughness factor calculated with the Hurst method on profiles, shown for the average of the two directions

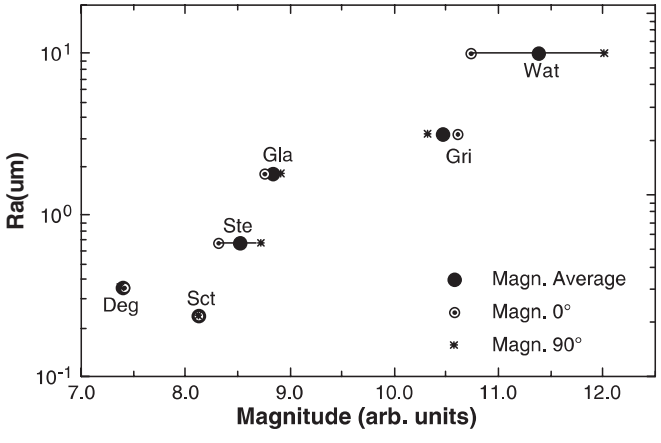

Fig. 8. The correlation between arithmetic average deviation, R_a, and the intercept with the *y*-axis (magnitude) for the Fourier method

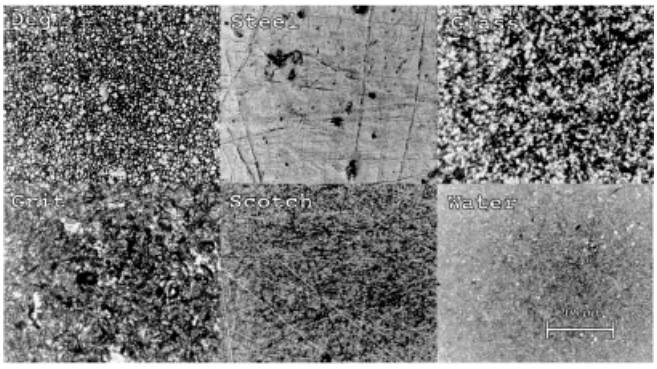

Fig. 9. Light-microscope images of the six samples, magnification 200×

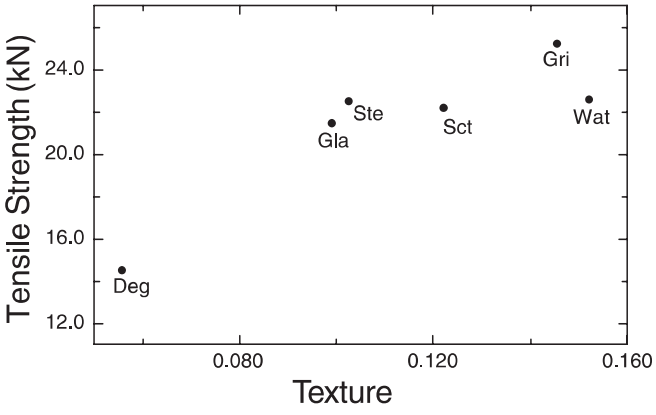

Fig. 10. Tensile strength versus texture from light-microscopy images, magnification 200×

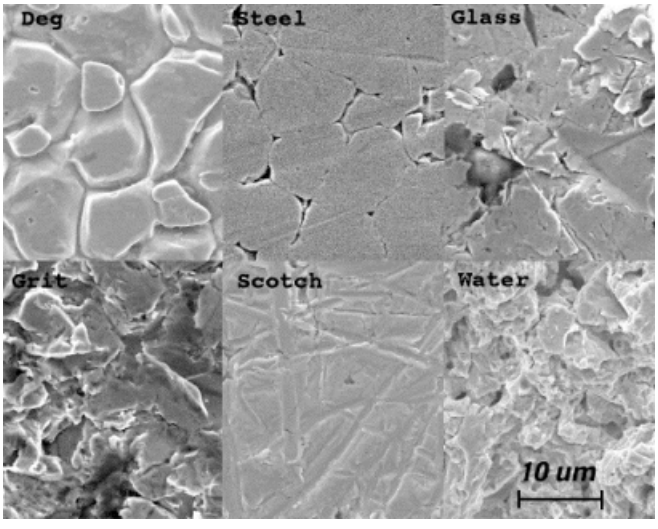

Fig. 11. SEM images of the six samples, 800× magnification, backscattered electrons

3.3 SEM profiles and Richardson plot

The samples were cut into slices and polished. Six to ten consecutive profile pictures, with a magnification of 3000× or 15 000×, were taken in the SEM and digitized. A threshold was applied to the pictures to obtain distinct black and white profiles, and they were added together to form one single profile. Figure 12 shows one example of a profile from the water-blasted sample and the corresponding scaling behavior.

The profile lengths were measured by a computer program, for different measuring sticks, and plotted in Richardson plots. The fractal dimensions were calculated and plotted versus tensile strength in Fig. 13. The degreased, Scotch-Brite, scrubbed and glass-blasted samples showed a similar relation between fractal dimension and tensile strength as for the profiler and LM images. The water- and grit-blasted samples deviated slightly and the steel-brushed sample showed a very low fractal dimension, lower than for the degreased sample. The explanation is probably that six to ten pictures, for each sample, is not statistically sufficient to give a good description of the overall surface and that a poor choice of profiles may severely alter the result.

The method is quite time consuming and not as convenient as the other methods. However, the fractal values should

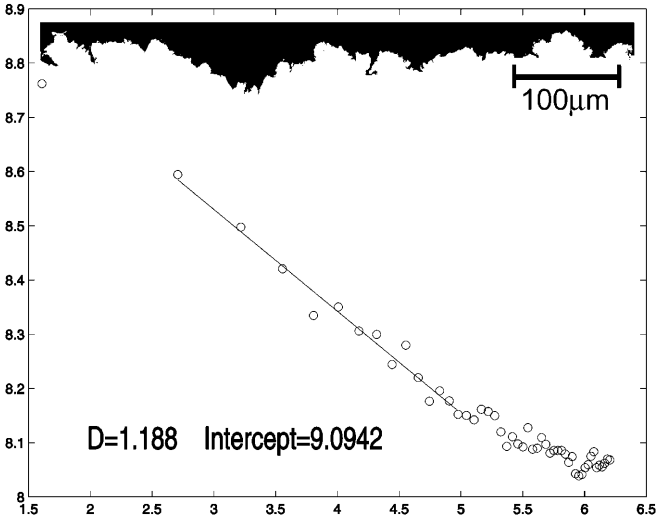

Fig. 12. An example of the scaling behavior for a profile cut from the water-blasted sample. In the inset six consecutive SEM images are added together and a threshold is applied to get a distinct profile. $D = 1.188$; intercept= 9.0942

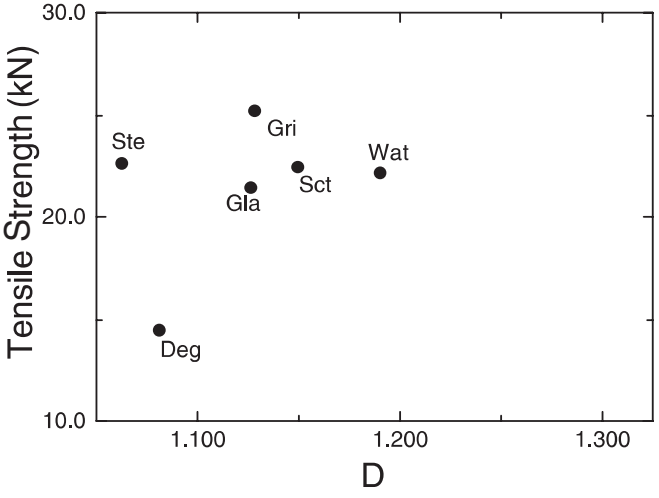

Fig. 13. Tensile strength versus fractal dimension for the Richardson method on SEM profiles. Note the different scale for D compared to the figures of the profiler data

be close to the real fractal dimension for the profiles, if statistical sufficiency can be achieved. The reason is that D is calculated according to the definition of fractal dimension and that SEM profiles reveal 'overhang' and other intricate structures, which cannot be seen by scanning or scattering techniques. It should also be easy to extract an upper and lower fractal cutoff that could be used together with the fractal dimension to decide the roughness factor. The change in wettability or contact angle could then be calculated from (1).

3.4 Atomic force microscopy

A Nanoscope II (Digital Instruments) equipped with a 15-μm scanner and standard pyramidal Si_3N_4 tips, was used to collect topographic images of the surfaces. Due to the limited vertical z-range of the piezo tube scanner, only the smoother samples such as the degreased and brushed samples, were flat enough to be scanned. However, areas of the blasted samples could be scanned if the flattest platelets caused by the blasting process were chosen. This did not give a statistical representation of the sample surface, but at least the nano-structure for the platelets could be investigated. We used scan sizes between 5000×5000 nm and $15\,000 \times 15\,000$ nm. Six typical AFM images are shown in Fig. 14.

The methods showed no connection between fractal dimension and tensile strength. The fractal behavior, for the *rms* method, was low compared to the Fourier method. This suggests that the *rms* method is more vulnerable to erroneous data than the Fourier method, Fig. 15.

The surface roughness of the brushed samples may be a mixture of two or more physical processes at that length-scale, rolling and brushing, giving rise to a mixture in fractal dimension. However, comparing the result with the other samples, using the Fourier method, suggests that all samples at that length-scale may be the result of (Brownian) random processes, as they are close to 2.5 in fractal dimension. The reason for values lower than 2.5 is probably due to the scanning-tip biasing the fractal dimension. This has been shown on simulated surfaces, where fractal dimensions calculated from AFM images are underestimated for the structure function and *rms* method, especially for higher fractal dimensions and when the tip dimensions are comparable with the magnitude of the surface roughness [14].

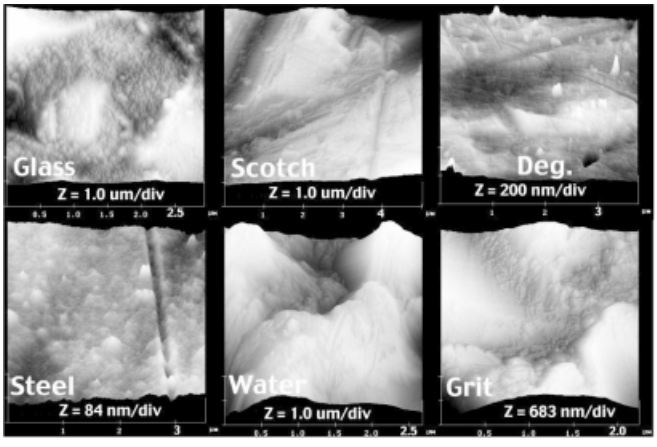

Fig. 14. AFM surface plots of the six samples. Note the crater caused by the glass-blasting process and the difference in image sizes

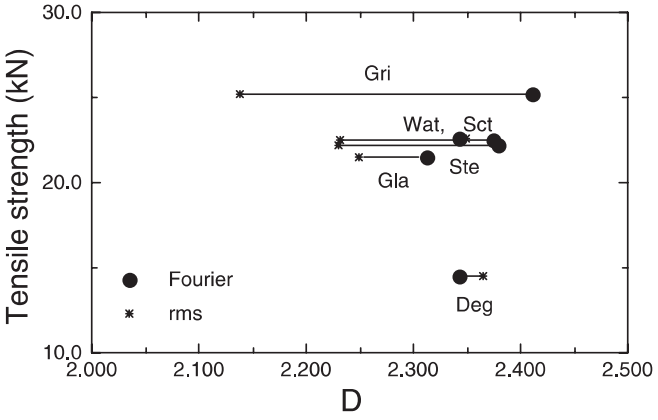

Fig. 15. Tensile strength versus fractal dimension calculated from AFM images, using the Fourier method and the *rms* method. The fractal dimensions were calculated from $4-6$ images and the bars reflect the difference between the two methods

4 Summary and conclusions

We have investigated the relationship between fractal dimension, evaluated by five fractal algorithms, and the tensile strength for six surface-treated steel samples. Four surface-analysis methods, profiler, AFM, SEM and LM, were used to collect profiles and image data. The fractal dimension varied considerably between the different methods and length-scales, but the overall relation between fractal dimension and tensile strength was qualitatively the same, except for the SEM images. The AFM was excluded from this comparison due to scanning limitations.

When we looked at profile data, the Fourier method and the Hurst method showed a high correlation between fractal dimension and tensile strength, with an offset in fractal dimension of 0.25 between the methods. Moreover, the roughness factor (related to wettability), calculated from the Hurst method, showed a correlation to tensile strength. So did the *rms* method, but the result was less clear. The SEM profiles turned out to be fractal, but their fractal dimensions did not correlate to tensile strength. Further, the R_a parameter was shown to correlate to the magnitude of the surface, and not to fractal dimension, hence demonstrating that R_a tells us little about the spatial distribution of the elevation data.

When looking at image data, only the texture values from the LM images could be related to tensile strength. The SEM images showed only weak fractal behavior.

Our results prove that tensile strength is correlated to roughness, although only at the length-scale of the profiler and with the LM method (0.5–100 μm), and that fractal analysis is necessary to extract this correlation. Traditional parameters, such as R_a and *rms*, fail to quantitatively characterize the surface roughness, and surface roughness at different length-scales contributes differently to the adhesion process and to the tensile strength. Therefore, microscopic methods have to be carefully chosen as they probe different length-scales. However, since the steel-treated samples showed relatively equal tensile strengths, only qualitative conclusions connecting fractal dimension and tensile strength could be made. Therefore, the challenge for the future is to use calibrated fractal methods and to manufacture surfaces with dis-

tinct fractal parameters, hence quantitatively correlating fractal dimension and magnitude to tensile strength.

Acknowledgements. The authors are grateful to Dr. N. Almqvist for fruitful discussions, and Nordbanken and the Kempe and LKAB Foundations for funding for the STM/AFM instrument. This work was performed partly under Contract 94-145 of the Swedish Research Council for Engineering Sciences.

References

1. J. Comyn: *Adhesion Science* (The Royal Society of Chemistry, Cambridge 1997)
2. J.C. Russ: J. Comput.-Assisted Microsc. **3**, 161 (1990)
3. C. Weiping, X. Chienghui: J. Mat. Sci. Lett. **16**, 113 (1997)
4. A. Shigeyasu, H. Tohru: Surf. Coatings Technol. **102**, 132 (1998)
5. R.D. Hazlett: J. Coll. Interf. Sci. **137**, 527 (1990)
6. S. Shibuichi, T. Yamamoto, T. Onda, K. Tsujii: J. Coll. Interf. Sci. **208**, 287 (1998)
7. S. Shibuichi, T. Onda, N. Satoh, K. Tsujii: J. Phys. Chem. **100**, 19512 (1996)
8. J.C. Russ: *Fractal Surfaces* (Plenum Press, New York 1994) pp. 27–244
9. J.M. Gómez-Rodriguez, A.M. Baró, L. Vázquez, R.C. Salvarezza, J.M. Vara, A.J. Arvia: J. Phys. Chem. **96**, 347 (1992)
10. P.I. Oden, A. Majumdar, B. Bhushan, A. Padmanabhan, J.J. Graham: J. Tribol. **114**, 666 (1992)
11. J.M. Williams, T.P. Beebe Jr.: J. Phys. Chem. **97**, 6249 (1993)
12. L. Vázquez, R.C. Salvarezza, P. Ocón, P. Herrasti, J.M. Vara, A.J. Arvia: Phys. Rev. E **49**, 1507 (1994)
13. J. Krim, I. Heyvaert, C. van Haesendonch, Y. Bruynseraede: Phys. Rev. Lett. **70**, 57 (1993)
14. B.B. Mandelbrot: *The Fractal Geometry of Nature* (Freeman, San Francisco 1982) p. 135
15. S. Talibuddin, J.P. Runt: J. Appl. Phys. **76**, 5070 (1994)
16. N. Almqvist: Surf. Sci. **355**, 221 (1996)
17. A. Mannelquist, N. Almqvist, S. Fredriksson: Appl. Phys. A **66**, 891 (1998)
18. E.L. Church: Appl. Opt. **27**, 1518 (1988)
19. J. Feder: *Fractals* (Plenum Press, New York 1988) p. 103
20. R.F. Voss, D. Saupe: *The Science of Fractal Images*, ed. by H.D. Peitegen, D. Saupe (Springer, New York 1988) pp. 22–113
21. E.L. Church: Proc. SPIE **680**, 102 (1986)